Applied Surface Science 257 (2011) 10715–10720

Contents lists available at ScienceDirect

Applied Surface Science

journal homepage: www.elsevier.com/locate/apsusc

Study of effect annealing temperature on the structure, morphology and photocatalytic activity of Si doped TiO_2 thin films deposited by electron beam evaporation

Zhongdan Lu, Xiaohong Jiang*, Bing Zhou, Xiaodong Wu, Lude Lu

Key Lab of Soft Chemistry and Functional Materials of Ministry of Education, Nanjing University of Science and Technology, Xiaolingwei 200, Nanjing 210094, China

ARTICLE INFO

Article history:
Received 31 March 2011
Received in revised form 9 July 2011
Accepted 19 July 2011
Available online 23 July 2011

Keywords:
Si doped TiO_2 thin films
Electron beam evaporation
Annealing
Photocatalytic activity

ABSTRACT

Transparent Si-doped TiO_2 thin films (Si-TiO_2) were deposited on quartz glasses using electron beam evaporation (EBE) and annealed at different temperature in an air atmosphere. The structure and morphology of these films were analyzed by X-ray diffraction (XRD), Raman microscopy (Raman), X-ray photoelectron spectroscopy (XPS) and atomic force microscopy (AFM). Meanwhile the photocatalytic activity of the films has also been evaluated on the basis of the degradation degree of rhodamine B in aqueous solution. Our experimental results suggest that the annealing temperature impact a strong effect on the structure, morphology and photocatalytic activity of Si-TiO_2 thin films. Furthermore the enhanced thermal stability of Si-TiO_2 films enabled them to elevate the phase transformation temperature of TiO_2 from anatase to rutile and enhanced the photocatalytic efficiency.

1. Introduction

Over past few years, TiO_2 thin films have attracted much attention due to their various applications ranging from the purification of toxic compounds in polluted water and air under the irradiation of ultraviolet (UV) light [1–4], dyes for sensitized solar cells [5–7], self-cleaning surfaces [8–11], to materials utilizing their photo induced super-hydrophilic properties [12]. It is well known that TiO_2 has three different phases, namely anatase, rutile and brookite, but anatase films exhibit the best photocatalytic activity. Unfortunately, the large scale application of TiO_2 thin film as mutual photocatalyst is hampered by the wide band-gap and higher recombination rate of photo-generated electrons and holes. Therefore, great efforts have been paid to improve the photocatalytic activity of TiO_2 thin films. Up to now, one of the most efficient strategies is to dope the films with nonmetallic and metallic species, such as Fe, Cu, Al, Ag, N, S, and Si [13–18]. Lots of work was dedicated to prepare TiO_2 thin films fabricated from sol–gel [19], chemical vapor deposition [20], magnetron sputtering [21] and electron beam evaporation [22]. Herein, electron beam evaporation method was utilized taking into account of its merits such as high deposition rate, facile controllability and excellent economy and practicability. However, the thus-obtained films are largely in amorphous state since the substrate is not heated during the overall process [22]. As a result, post-deposition annealing becomes one of the key pathways in controlling the structure, morphology and thereafter photocatalytic activity of these films.

In this work, the TiO_2 and Si-TiO_2 targets have been simply prepared and the corresponding films were deposited on quartz glass substrates by electron beam evaporation and annealed in an air atmosphere. The effect of annealing temperatures on phase transition, the structure and surface morphology of Si-TiO_2 thin films has been investigated. The photocatalytic activity of TiO_2 and Si-TiO_2 thin films was examined on the degree of degradation of rhodamine B in aqueous solution with UV illumination.

2. Experimental

2.1. Preparation of TiO_2 and Si-TiO_2 targets

The TiO_2 and Si-TiO_2 targets were prepared with the titanium oxide (99.9% pure) and 3% silica powder (99.9% pure) doping in TiO_2 powder which were tabletted using universal testing machine under high pressure and sintered using a muffle furnace at 1000 °C.

2.2. Preparation of TiO_2 and Si-TiO_2 films

Transparent TiO_2 and Si-TiO_2 thin films were deposited on quartz glasses (25 mm × 10 mm × 1 mm) using electron beam evaporation method. The distance from the target to the substrate is about 400 mm. Before deposition, the quartz glass substrates were respectively rinsed with acetone and ethanol under

* Corresponding author at: Tel.: +86 25 84315943; fax: +86 25 84315054.
E-mail address: jiangxh24@mail.njust.edu.cn (X. Jiang).

0169-4332/$ – see front matter © 2011 Elsevier B.V. All rights reserved.
doi:10.1016/j.apsusc.2011.07.085

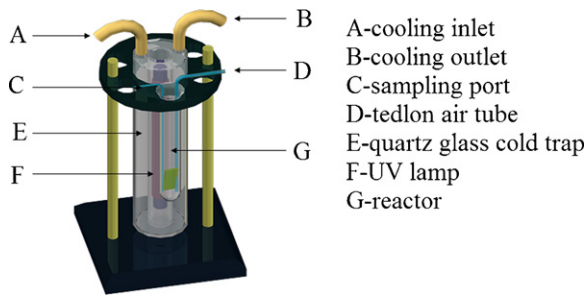

Fig. 1. The schematic diagram of the photocatalytic reactor.

ultrasonication for 15 min and then rinsed thoroughly with deionized water. When the base pressure of 5×10^{-3} Pa, the substrates are first pre-sputtered in an argon atmosphere for 5 min. The working pressure for deposition is 4×10^{-3} Pa, with an electron beam flow of 0.08 A. The electron gun voltage is 8.0 kV and the current is 800 mA. The depositing time of all films keeps being 60 min. The deposited films are then annealed at different temperatures for 4 h in an air atmosphere.

2.3. Characterization of TiO_2 and Si-TiO_2 films

The crystal structures of these films were analyzed by X-ray diffraction (Bruker D8 Superspeed) using Cu K_α source under a voltage of 40 kV, and Raman microscopy (Renishaw inVia) with a laser wavelength of 514.5 nm. The chemical composition of these films was determined by X-ray photoelectron spectroscopy (Thermo Fisher K-Alpha) with an Al K_α source. All the binding energies are referenced to C1s peak at 285 eV. The surface morphologies were characterized by an atomic force microscopy (Seiko Instruments Inc., SPI-3800). The thickness of these films, as measured by a step device (Ambios Technology XP-2), is approximately 400 nm. All targets and films were annealed using a muffle furnace (Thermo Scientific Lindberg/Blue M BF51866C).

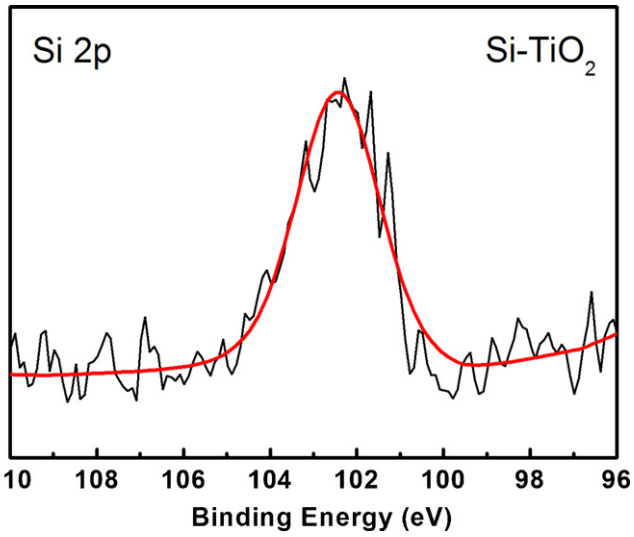

Fig. 3. XPS spectra of Si elements on the surface of Si-TiO_2 thin film annealed at 500 °C.

2.4. Photocatalytic activity of TiO_2 and Si-TiO_2 films

The optical transmittance spectra, in the range of 200–800 nm, were recorded on a UV-Visible spectrophotometer using a blank substrate as reference (UV-2001). The photocatalytic property of

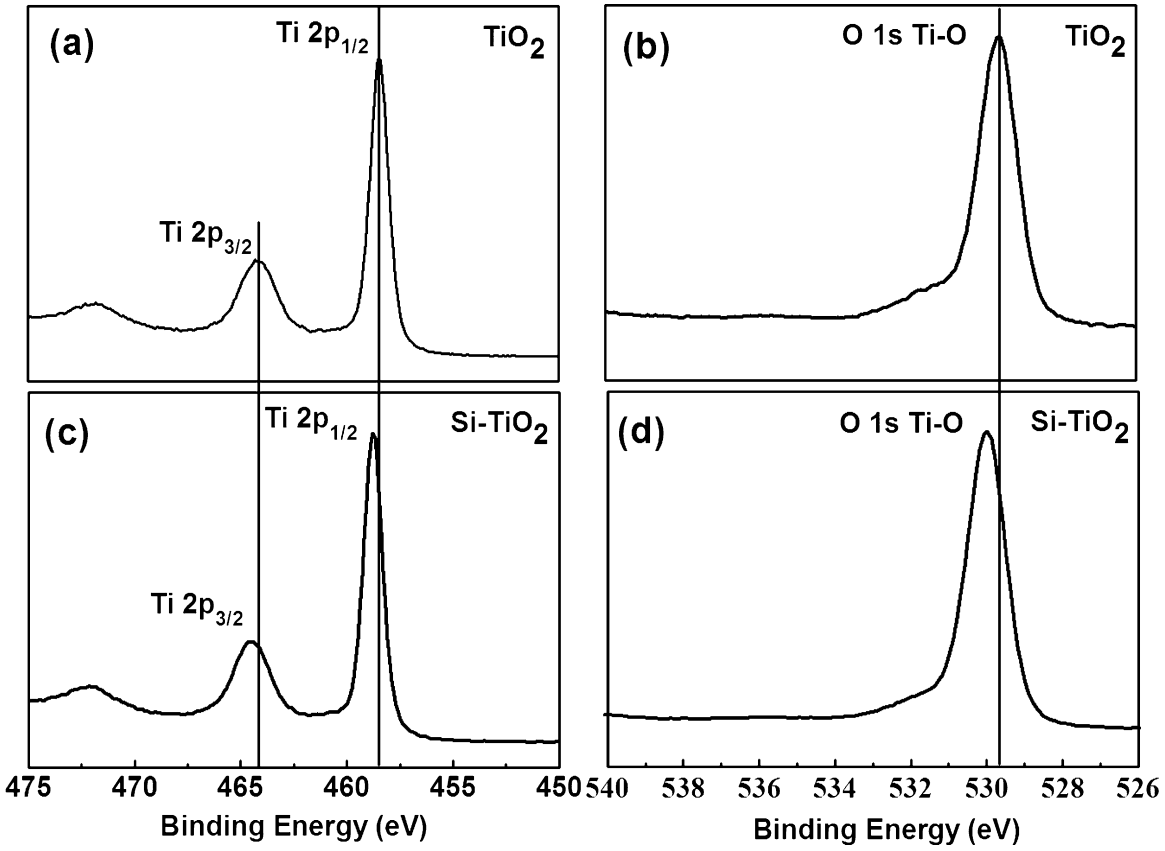

Fig. 2. XPS spectra of Ti, O elements on the surface of the films annealed at 500 °C: TiO_2 thin film (a, b); Si-TiO_2 thin film (c, d).

Table 1
The XRD data of Si-TiO_2 films annealed at different temperatures.

Annealing temperature of Si-TiO: films (°C)	β	2θ (°)	D (nm)		ε	
			A101	R110	A101	R110
500	0.300	25.49	26.9		0.33	
600	0.255	25.42	31.6		0.28	
700	0.209	25.48	38.5		0.23	
800	0.129	27.55		62.7		0.13
900	0.122	27.45		66.3		0.12

the prepared thin films was evaluated by measuring the photodecomposition yield of rhodamine B solution (the absorption spectra at 553.5 nm) at an initial concentration of 10 mg/L. The films with a size of 2.5 cm^2 were immersed in the solution in a tubular quartz reactor while illuminating with a mercury lamp (300 W) which characteristic wavelength is 365 nm (Fig. 1).

3. Results and discussion

3.1. Chemical composition analysis

The chemical composition of the TiO_2 and Si-TiO_2 films, annealed at 500 °C, is determined by XPS (Fig. 2). It can be seen that elements including Ti, O, C, and Ti, O, Si, C can be observed for TiO_2 and Si-TiO_2 deposited films respectively. The appearance of pho-

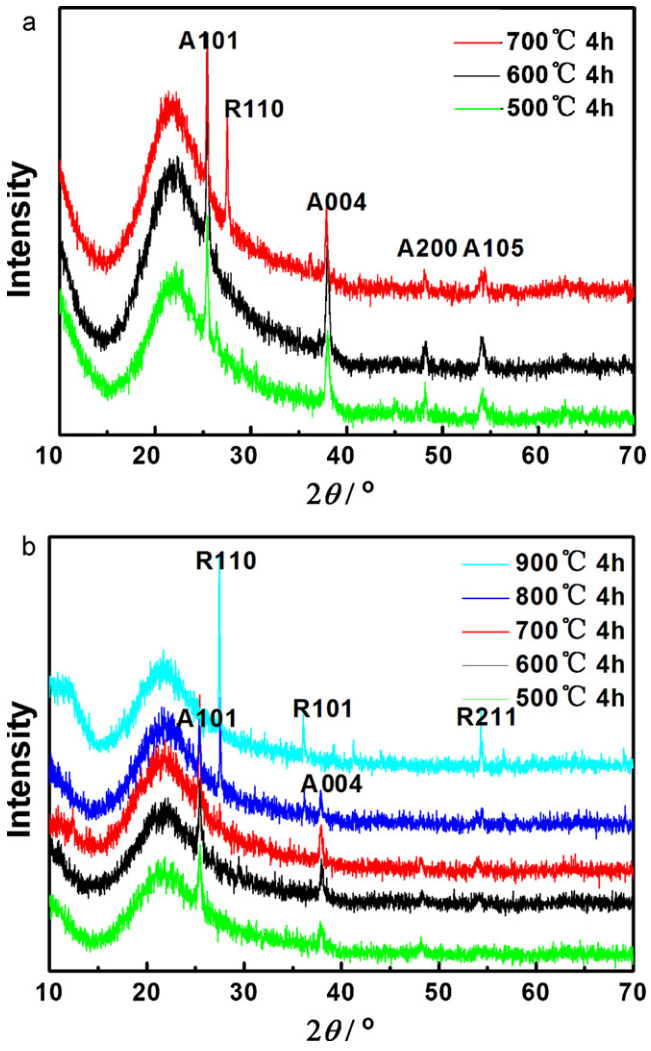

Fig. 4. XRD patterns of TiO_2 thin films (a) and Si-TiO_2 thin films (b).

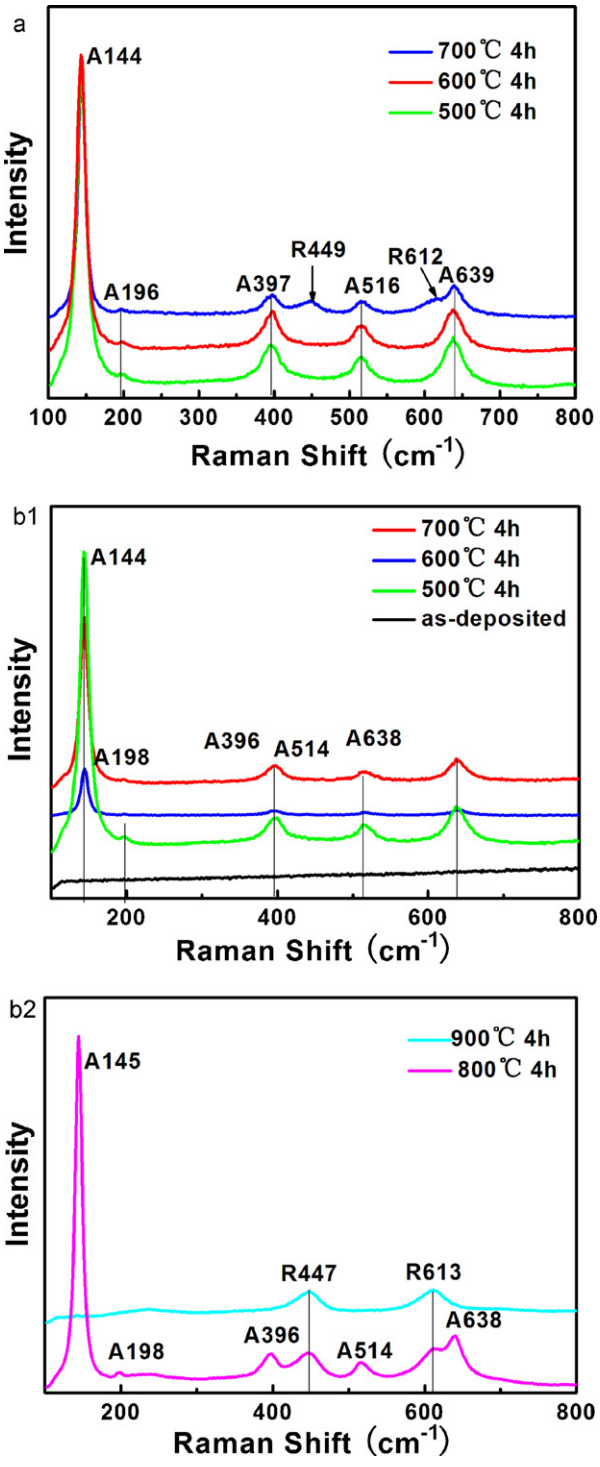

Fig. 5. Raman spectra of TiO_2 films (a) and Si-TiO_2 films (b, c).

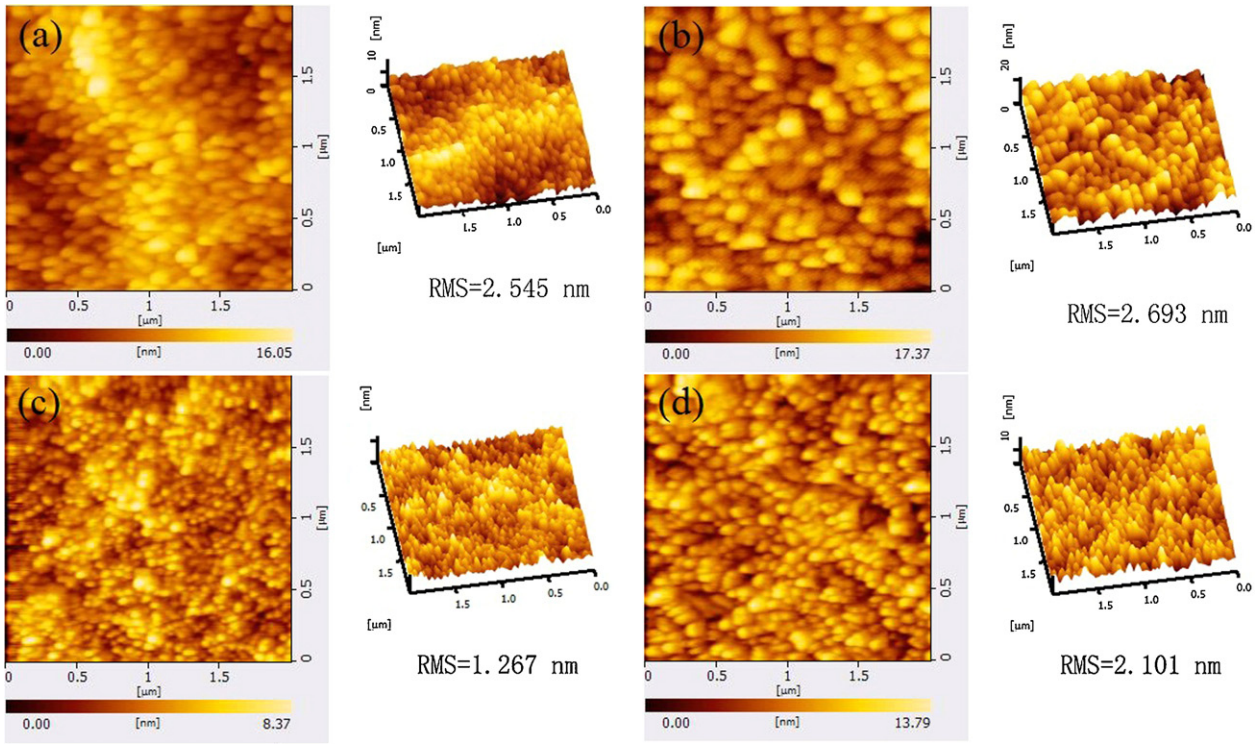

Fig. 6. Typical AFM images of these films annealed at 600 °C and 700 °C: TiO_2 films (a, b); Si-TiO_2 films (c, d).

toelectron peak for Ti $2p_{1/2}$ and Ti $2p_{3/2}$ at 458.43 and 464.28 eV and the O1s peak at 529.65 eV from TiO_2 films reveal the presence of Ti^{4+} species as TiO_2. In contrast, the two peaks for Ti $2p_{1/2}$ and Ti $2p_{3/2}$ in Si-TiO_2 film shifts to 458.81 eV and 464.58 eV, and the O1s one moves to 530.03 eV, respectively. In addition, as showed in Fig. 3, the peak at 102.78 eV, close to the binding energy of Si 2p (103.1 eV) [23] in pure SiO_2, suggests the successful doping of SiO_2 in the prepared film. The decremented binding energy could be most likely due to the high electronegativity (the ability of an atom or a functional group in a molecule to attract electrons or electron density to itself and thus enhancing the tendency to form negative ions [24]) of Si (1.8) in relative to Ti (1.5), which leads silicon atoms to be more electron density and reduces the effective positive charge on the Si atoms formation of Si–O–Ti bond [25]. This is an indication of strong interaction of silicon atoms with TiO_2 lattice which possibly formed Si–O–Si and/or the Si–O–Ti bonds.

3.2. Crystal structural analysis

Fig. 4 shows the XRD patterns of TiO_2 (a) and Si-TiO_2 thin films (b), which were annealed at different temperature for 4 h in an air atmosphere. Titanium dioxide in all films annealed at 500 °C, 600 °C are in anatase phase, characterized by the two major peaks centered at $2\theta = 25.4°$ and 37.8°, corresponding to (1 0 1) and (0 0 4) in anatase-TiO_2 respectively. The Si-TiO_2 thin film annealed at 700 °C is in anatase phase, as demonstrated by the three main peaks at $2\theta = 25.4°$, 37.8°, and 48.1°, respectively, which can be indexes to (1 0 1), (0 0 4) and (2 0 0) in anatase-titania. Interestingly, if the sample is annealed at a higher temperature, say 800 °C, the phase of Si-TiO_2 film turns into rutile. A complete transition occurs at 900 °C, as demonstrated clearly by the presence of three characteristic diffraction peaks at $2\theta = 27.5°$, 36.1°, and 54.3°. Owing to the low doping degree, neither peaks characteristic of SiO_2 nor clear peak movement of the characteristic peaks corresponding to anatase or rutile phases has been observed. It should be noted that the wide and broad signal at 22.1° originates from quartz glass.

Such annealing temperature-dependent phase transition can be also clearly demonstrated by Raman spectroscopy (Fig. 5). Specifically the shifts at around 144, 196, 397, 516, and 639 cm^{-1} in both TiO_2 and Si-TiO_2 films annealed at 500 °C, 600 °C, are in good agreement with the vibration modes of TiO_2 in anatase phase. Identical to the observation in XRD experiment, the peaks at about 142, 232, 447, and 613 cm^{-1} from rutile-TiO_2 come out for sample annealed at 800 °C. While they become predominant for films annealed at 900 °C. The enhanced phase transition for silicon doped TiO_2 films suggests their higher thermal stability.

The mean crystallite size (D) and the ratio of the crystal lattice distortion (ε) of the films at different temperature were evaluated by the following equations [26,27]:

$$D = \frac{0.9\lambda}{\beta \cos\theta} \quad (1)$$

$$\beta \cos\theta = \frac{\lambda}{D} + 4\varepsilon \sin\theta \quad (2)$$

Wherein λ and β correspond to the irradiation wavelength (1.54 nm in this case) and the full width at half maximum of the strongest diffraction peak. ε and θ are the ratio of the crystal lattice distortion and the Bragg angle of the most intense peak at a specific phase.

The crystallite sizes of the TiO_2 thin films, annealed at 500 °C, 600 °C, and 700 °C, are in the order of 34.4, 41.5 and 46.3 nm, respectively. In contrast, the sizes of Si doped films, annealed at 500 °C, 600 °C, 700 °C, 800 °C, and 900 °C, are in 26.8, 31.6, 38.5, 62.7 and 66.3 nm, respectively (Table 1). The increased crystallite sizes for TiO_2 and Si-TiO_2 films at elevated annealing temperature can be attributed to the thermal instability of nano-particals. On the other hand, the crystallite sizes of the Si-TiO_2 films are smaller than those of TiO_2 ones, which may be related to the smaller radius of silicon. In addition, the ratios of the crystal lattice distortion of the Si-TiO_2 films decrease with the incremental of the annealing temperature.

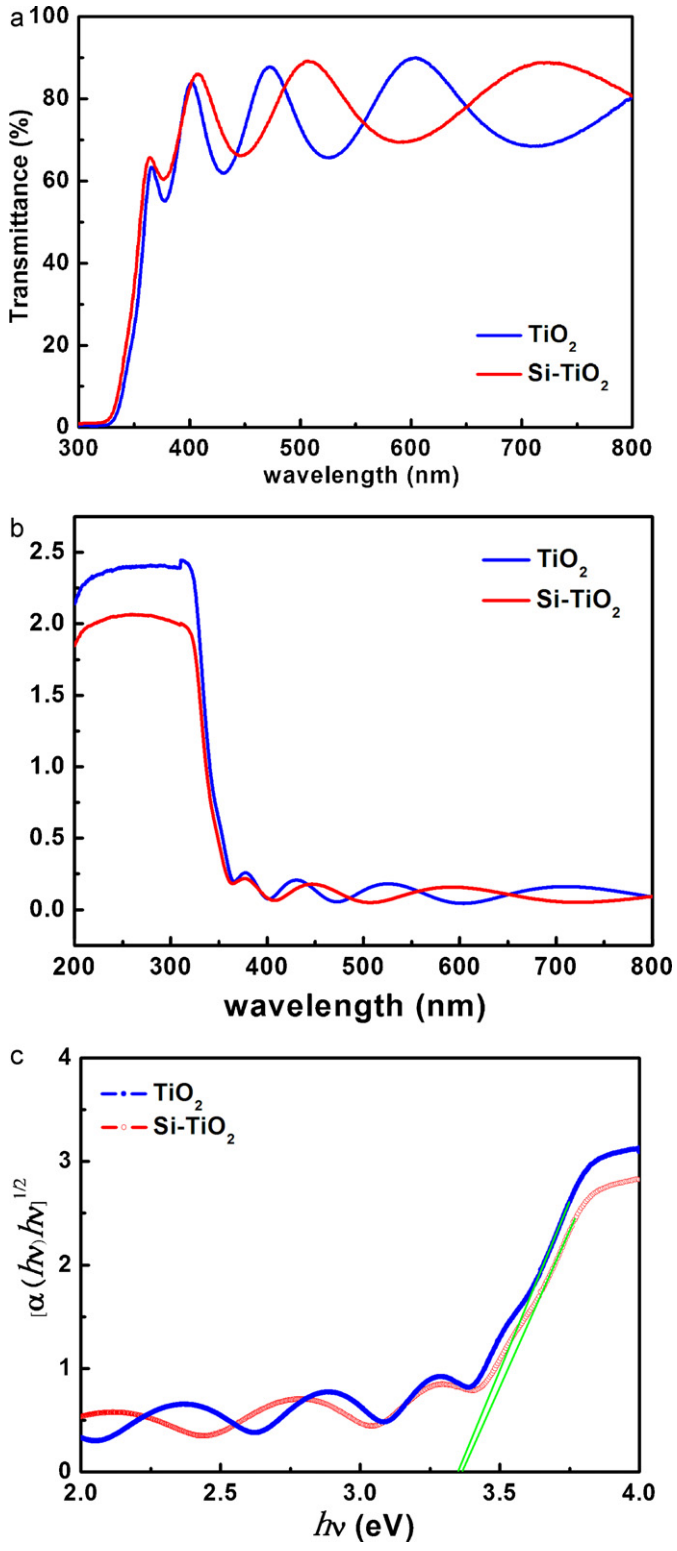

Fig. 7. UV–Vis of TiO_2 and Si-TiO_2 films annealed at 500 °C: (a) transmittance spectra; (b) absorption spectra; (c) band gap spectra.

3.3. Morphology evaluation

Fig. 6 displays typical AFM images of TiO_2 and Si-TiO_2 thin films annealed at 600 °C and 700 °C, respectively. It can be seen that these films are quite uniform. In compared with TiO_2 thin films, the surfaces grain sizes and the average surface roughness of Si-TiO_2 ones decrease. However the particle sizes of all films increase

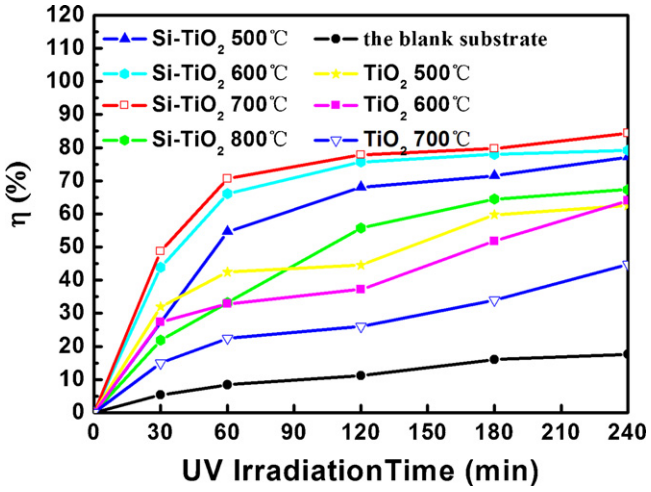

Fig. 8. Photo-degradation of rhodamine B with TiO_2 and Si-TiO_2 thin films annealed at different temperature.

at elevated annealing temperature. These results are in agreement with the results from XRD. All our experiments demonstrate unambiguously that the annealing temperature is of great essential for manipulating the surface morphologies of TiO_2 and Si-TiO_2 thin films.

3.4. Transmittance measurement

As illustrated in Fig. 7, the transmittance of TiO_2 and Si-TiO_2 films deposited on quartz glasses annealed at 500 °C, are more than 70% of wavelength in the region of 300–800 nm. The transmittance of Si-TiO_2 film is higher than that of TiO_2 film. Additionally, a significant blue-shift of the absorption for Si-TiO_2 film in relative to TiO_2 film can be observed in UV–Vis spectra. For example, the absorption edges of TiO_2 and Si-TiO_2 films annealed at 500 °C, attributed to the quantum size effects, appear at 365.37 and 362.49 nm, respectively.

The band-gap energy (E_g) of the indirect transition of the films, on the basis of the UV–Vis absorption edge, can be calculated from the following equation [28]:

$$\alpha h\nu = B_i(h\nu - E_g)^2 \quad (3)$$

Herein α and B_i correspond to the absorption constant and the constant for an indirect transition which does not depend on photon energy respectively. Whereas $h\nu$ and E_g represent the energy of the photon and that of the band gap. The indirect band gap can be derived directly from the crosspoint of extended line for the linear domain with the axis in the plot of $(\alpha h\nu)^{1/2}$ versus $h\nu$. The calculated band gap energies of the TiO_2 and Si-TiO_2 films annealed at 500 °C are 3.34 and 3.36 eV, respectively.

3.5. Photocatalytic activities and mechanism

The photocatalytic activities of these films were carried out on the determination of the degradation process of rhodamine B solution. The decomposition yield (η) can be estimated by the equation:

$$\eta = \frac{A_0 - A_t}{A_0} \times 100\% \quad (4)$$

where A_0 and A_t are absorptions at the initial and a fixed period of time interval of the reaction system. Fig. 8 illustrates the transition tendency of rhodamine B under photo-degradation catalyzed by TiO_2 and Si-TiO_2 thin films. Compared with the blank sample, the degradation rate of rhodamine B in the presence of TiO_2 thin film is increased significantly. Moreover the photocatalytic activities of the Si-TiO_2 films become superior to those of TiO_2 ones

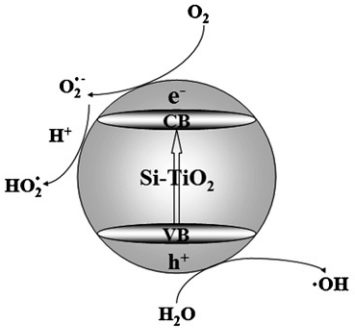

$$TiO_2 + h\nu \rightarrow e^- + h^+ \quad (5)$$

$$h^+ + OH^-(H_2O) \rightarrow {}^{\bullet}OH + H^+ \quad (6)$$

$$e^- + O_2 \rightarrow O_2^{\bullet -} \quad (7)$$

$$O_2^{\bullet -} + H^+ \rightarrow {}^{\bullet}HO_2 \quad (8)$$

$$h^+(\text{and/or } {}^{\bullet}OH \text{ and/or } {}^{\bullet}HO_2) + RhB \rightarrow \text{intermedicated products} \rightarrow CO_2 + H_2O + NO_3^- + NH_4^+ \quad (9)$$

Fig. 9. The schematic diagram of UV light photocatalytic mechanism.

after a 4-h-period of UV-illumination at the same annealing temperature. This could be arising from the reduced photo-generated electron and holes recombination rate in Si doped system upon illumination. For samples annealed at diffident temperatures, the Si-TiO_2 film annealed at 700 °C exhibit the highest photocatalytic efficiency, which can induce a maximum degradation degree of 84.37% higher than SiO_2–TiO_2 composite films using sol–gel by UV light (500 W) [29]. In addition, the similar results were reported in Si-TiO_2 nanotube using CVD by UV light (300 W) [30].

Fig. 9 displays the schematic diagram of UV light photocatalytic mechanism. When the TiO_2 films were irradiated by UV light, the electrons (e^-) were excited and transited from valence band (VB) to the conduction band (CB), while leaving electron holes (h^+) in the valence band (Eq. (5)). They can move to TiO_2 films surface and the holes were scavengered by the hydroxides on the surface to produce the hydroxyl radicals (•OH) (Eq. (6)). The electrons react with dissolved oxygen to produce superoxide radical anions ($O_2^{\bullet -}$) and peroxide ($HO_2^{\bullet}$) which can be participated in the oxidation–reduction reaction (Eqs. (7) and (8)) [31]. Furthermore, rhodamine B was degraded by the h^+ (•OH) and $O_2^{\bullet -}$ as shown in Eq. (9) [32]. In addition, the movement of the electrons in Si-TiO_2 film was slower than that of TiO_2 film and some electrons contacting with silicon can be attracted. Meanwhile, the increment in band gap energy causes a lowering in the energy of the valence band and an increase in the conduction band edge which will result in the reduction of the recombination rate of electron–hole pairs generated during the UV illumination, thereby promoting the photocatalytic activity accordingly [33].

4. Conclusions

Both TiO_2 and Si-TiO_2 thin films have been deposited on quartz glasses using electron beam evaporation method. Doping of Si in TiO_2 film improves the thermal stability which results in an enhanced phase transition temperature of TiO_2 from anatase to rutile phase. The photocatalytic activities for the degradation of rhodamine B of Si-TiO_2 thin films are higher than those of the counterparts in undoped ones. After doping, the band gap of TiO_2 increases owing to the reduction of the photo-generated electron and holes recombination rate under illumination, and therefore allows for the improvement of the photocatalytic efficiency.

Acknowledgments

This work was supported by the National Natural Science Foundation of China (50972059), 2010–2012 Intergovernmental Cooperation Projects in Science and Technology of the Ministry of Science and Technology of PRC (nos. 5 and 6), Science and Technology Developing Item of Nanjing city (200901061).

References

[1] M. Takeuchi, S. Sakai, M. Matsuoka, M. Anpo, Res. Chem. Intermed. 35 (2009) 973–983.
[2] A. Eshaghi, R. Mozaffarinia, M. Pakshir, A. Eshaghi, Ceram. Int. 37 (2011) 327–331.
[3] F.M. Meng, X.P. Song, Z.Q. Sun, Vacuum 83 (2009) 1147–1151.
[4] M.W. Pyuna, E.J. Kimb, D.-H. Yooc, S.H. Hahna, Appl. Surf. Sci. 257 (2010) 1149.
[5] J. Xua, L. Wang, G.J. Liang, Z.K. Bai, L. Wang, W.L. Xu, X.L. Shen, Spectrochim. Acta Part A 78 (2011) 287–293.
[6] J.C. Zhang, X. Zheng, X.Y. Liang, W.L. Cao, J. Inorg. Organomet. Polym. 21 (2011) 150–156.
[7] V. Senthilkumar, M. Jayachandran, C. Sanjeeviraja, Thin Solid Films 519 (2010) 991–994.
[8] D. Ollis, Catal. Appl. B 99 (2010) 478–484.
[9] X.T. Zhang, A. Fujishima, M. Jin, A.V. Emeline, T. Murakami, J. Phys. Chem. B 110 (2006) 25142–25148.
[10] K. Katsumata, S. Okazaki, C.E.J. Cordonier, T. Shichi, T. Sasaki, A. Fujishima, ACS Appl. Mater. Interfaces 2 (2010) 1236–1241.
[11] U. Cernigoj, M. Kete, U.L. Stangar, Catal. Today 151 (2010) 46–52.
[12] P. Eiamchai, P. Chindaudom, M. Horprathum, V. Patthanasettakul, P. Limsuwan, Mater. Des. 30 (2009) 3428–3435.
[13] B. Zhou, X.H. Jiang, R.Q. Shen, L.D. Lu, A.V. Rogachev, J. Nanjing Univ. Sci. Technol. (Nat. Sci.) 34 (2010) 547–552.
[14] B. Wang, Q. Li, W. Wang, Y. Li, J.P. Zhai, Appl. Surf. Sci. 257 (2011) 3473–3479.
[15] P. Sangpour, F. Hashemi, A.Z. Moshfegh, J. Phys. Chem. C 114 (2010) 13955–13961.
[16] M. Yoshinaga, K. Yamamoto, N. Sato, K. Aoki, T. Morikawa, A. Muramatsu, Catal. Appl. B 87 (2009) 239–244.
[17] G. Sauthier, F.J. Ferrer, E. György, Thin Solid Films 519 (2010) 1464–1469.
[18] D. Lee, D. Omolade, R.E. Cohen, M.F. Rubner, Chem. Mater. 19 (2007) 1427–1433.
[19] I. Moriguchi, H. Maeda, Y. Teraoka, S. Kagawa, Chem. Mater. 9 (1997) 1050–1057.
[20] P.M. Parthangal, M.R. Zachariah, Chem. Mater. 17 (2005) 3830–3836.
[21] S.H. Kang, J.W. Lim, H.S. Kim, J.Y. Kim, Y.H. Chung, Y.E. Sung, Chem. Mater. 21 (2009) 2777–2788.
[22] S.S. Lin, Y.H. Hung, S.C. Chen, J. Nanosci. Nanotechnol. 9 (2009) 3599–3605.
[23] Y.S. Zhang, H.B. Yin, A.L. Wang, M. Ren, Z.M. Gu, Y.M. Liu, Y.T. Shen, L.B. Yu, T.S. Jiang, Appl. Surf. Sci. 257 (2010) 1351–1360.
[24] A.D. McNaught, A. Wilkinson, Blackwell Science, 2nd ed., 1997.
[25] S.J. Iwamoto, S. Iwamoto, M. Inoue, Chem. Mater. 17 (2005) 650–655.
[26] S.A. Amin, A. Hosseinnia, M. Pazouki, Powder Technol. 196 (2009) 241–245.
[27] G.K. Williamson, W.H. Hall, Acta Metall. 1 (1953) 22–31.
[28] N. Serpone, D. Lawless, R. Khairutdinovt, J. Phys. Chem. 99 (1995) 16646–16654.
[29] H. Yang, Q.H. Shen, S. Li, J.J. Zong, Y. Zhu, Rare Met. Mater. Eng. 39 (2010) 280–283.
[30] Y. Su, S. Chen, X. Quan, H.M. Zhao, Y.B. Zhang, Appl. Surf. Sci. 255 (2008) 2167–2172.
[31] T.S. Natarajan, M. Thomas, K. Natarajan, H.C. Bajaj, R.J. Tayade, Chem. Eng. J. 169 (2011) 126–134.
[32] S. Horikoshi, H. Hidaka, N. Serpone, Environ. Sci. Technol. 37 (2003) 5813–5822.
[33] P. Periyat, K.V. Baiju, P. Mukundan, P.K. Pillai, K.G.K. Warrier, Appl. Catal. A: Gen. 349 (2008) 13–19.